

This is the preprint of the contribution published as:

Hari, V., **Rakovec, O.**, Zhang, W., Koppa, A., Collins, M., **Kumar, R.** (2024):
On the role of the Atlantic Meridional Mode in eastern European temperature variability
Atmos. Res. **297** , art. 107082

The publisher's version is available at:

<https://doi.org/10.1016/j.atmosres.2023.107082>

On the role of the Atlantic Meridional Mode in Eastern European Temperature Variability

Vittal Hari^{a,g}, Oldrich Rakovec^{b,c}, Wei Zhang^d, Akash Koppa^e, Matthew Collins^f, Rohini Kumar^{b,g}

^a*Department of Environmental Science and Engineering, Indian Institute of Technology (ISM) Dhanbad, India*

^b*UFZ-Helmholtz Centre for Environmental Research, Leipzig, 04318, Germany*

^c*Faculty of Environmental Sciences, Czech University of Life Sciences Prague, Kamýcká 129, Praha – Suchbátka, 165 00, Czech Republic*

^d*Department of Plants, Soils and Climate, Utah State University, Utah, USA.*

^e*Hydro-Climate Extremes Lab (H-CEL), Faculty of Bioscience Engineering, Ghent University, Coupure links 653, 9000 Ghent, Belgium*

^f*Department of Mathematics and Statistics, University of Exeter, Exeter, UK*

^g*Corresponding authors*

Abstract

1 The eastern European (EE) region has experienced record-breaking heatwave events in
2 recent years, and such events are expected to increase in future with global warming.
3 Early warning systems are an important step towards mitigating their impacts. Here we
4 seek to further clarify the effect of Atlantic Meridional Mode (AMM) on the EE region
5 temperature variability. Using observations and climate model experiments, we show a
6 significant association between the AMM and temperature variability across the region.
7 The positive phase of AMM leads to a significant increase in EE temperature of 0.9°C, p-
8 value < 0.1, for a one standard deviation AMM anomaly, and vice-versa. The mechanism
9 through which the AMM can modulate the EE temperature arises through a persistent
10 planetary-scale Rossby wave which causes an anomalous anticyclone circulation leading to
11 a positive temperature anomaly. This relationship, along with the mutually exclusive and
12 independent large-scale climatic modes such as the El Niño–Southern Oscillation (ENSO)

13 and North Atlantic Oscillation (NAO), have important implications for improving the
14 prediction of EE heatwaves.

Key words: Eastern Europe, Heatwave, Atlantic Meridional Mode, Climate model
experiments.

15 **1. Introduction**

16 Since the beginning of the century, there has been a significant increase in the num-
17 ber of summer heatwaves in Europe [Robine et al., 2008; Otto et al., 2012; Meehl and
18 Tebaldi, 2004; Zhang et al., 2020] – which have had major impacts on local communities
19 [Alexander, 2011]. Some of the notable impacts due to such high temperatures include
20 air-quality degradation, forest fires [Earl and Simmonds, 2018], substantial crop yield loss
21 [Barriopedro et al., 2011], human mortality [Hari et al., 2022], and degradation of bio-
22 diversity [Welbergen et al., 2008]. The extreme heatwaves during the summers of 2003
23 and 2010, for example, were associated with premature deaths of nearly 70 000 people in
24 Europe [Robine et al., 2008] and 50 000 people in Russia [Otto et al., 2012], respectively.
25 Extreme temperatures associated with heatwaves over Europe are projected to increase
26 in the future at a the faster rate than the global mean temperature [Russo et al., 2015].
27 Therefore, the understanding of underlying physical triggers of such high impact events –
28 specifically over the Eastern European (EE) region – will significantly aid in adaptation
29 to extreme events.

30 A number of studies have identified physical mechanisms that trigger European heat-
31 waves [García-Herrera et al., 2010; Lhotka et al., 2018; Miralles et al., 2014; Schumacher

32 et al., 2019]. These studies indicate that land-atmosphere feedback mechanisms are impor-
33 tant aspects during these heatwaves. However, even though the major heatwaves – such
34 as 2003 at central European [Fischer et al., 2007] and 2010 event in the EE region [Mi-
35 ralles et al., 2019] – were strengthened due to land-atmosphere coupling, these events were
36 initiated by anomalous large-scale atmospheric circulations [Liu et al., 2020]. Typically, a
37 persistent anticyclonic circulation – favouring clear skies, air subsidence, and surface solar
38 heating [Liu et al., 2020; Li et al., 2020], that simultaneously reduces the zonal flow and
39 advection of warm air away from the region [Lhotka et al., 2018] – are the main features
40 associated with heatwaves over Europe [Brunner et al., 2018]. During the summer, the
41 EE region has a tendency towards the occurrence of these kinds of anticyclonic circulation
42 events [Tyrlis and Hoskins, 2008], and it is reported that many of the recent heatwaves over
43 the region were associated with such blocking conditions [Dole et al., 2011]. Moreover, it
44 is found that these long-lasting blocking conditions are related to quasi-stationary Rossby
45 waves [Dole et al., 2011; Di Capua et al., 2021; Strigunova et al., 2022]. Studies argue
46 that such mechanisms which trigger these stationary Rossby waves leading to heatwave
47 are connected to some of the known large-scale features such as, El Niño–Southern Os-
48 cillation (ENSO; Brönnimann [2007], Sun et al. [2016]), the North Atlantic ocean (NAO;
49 Hurrell [1995]; Krüger et al. [2020], Bierkens and Van Beek [2009], Cassou et al. [2005],
50 Della-Marta et al. [2007], Schubert et al. [2014]), Scandinavian pattern (Chen et al. [2019])
51 and also East Atlantic/Western Russia teleconnection (EAWR; Zhao et al. [2020]).

52 European climate is, in general, influenced by several important climatic modes – viz.,
53 ENSO and North Atlantic Oscillation (NAO; Hurrell [1995]; Krüger et al. [2020], Bierkens

54 and Van Beek [2009] Kautz et al. [2022]) and the atmospheric response of both of these cli-
55 matic modes to European climate closely resembles Toniazzo and Scaife [2006]. However,
56 the influence of both these dominant climate modes (ENSO and NAO) on the variability
57 of European climate is more pronounced during the winter season [Hurrell, 1995], and per-
58 haps their influence on the summer season is limited [Folland et al., 2009]. Nonetheless, a
59 recent study [Sun et al., 2016] showed that the influence of ENSO on the summer Euro-
60 pean Climate – specifically over the EE region – has strengthened significantly post-1980.
61 The theoretical linear baroclinic model suggests that the increasingly strong teleconnec-
62 tion between the summer ENSO and the EE region may be related to a change in the
63 tropical thermal forcing over the Pacific – which can excite an eastward propagation of the
64 Rossby wave reaching the EE region, causing the climatological changes [Sun et al., 2016].
65 Thus, these studies show that the ENSO and NAO profoundly influence EE temperature
66 variability. Nonetheless, apart from these climatic modes, disjoint studies [Trenberth and
67 Fasullo, 2012; Cassou et al., 2005] suggest that the anomalous diabatic heating over the
68 tropical Atlantic Ocean caused a heatwave over the EE region by forcing a quasi-stationary
69 Rossby wave during the summers of 2010 – and in general heatwave and droughts over
70 the Eurasian region [Schubert et al., 2014]. Having mentioned this, the effect of Atlantic
71 Meridional Mode (AMM) – a dominant climatic mode over the tropical Atlantic Ocean
72 [Chiang and Vimont, 2004] – has not been explored in existing literature. In addition,
73 Simmonds Simmonds [2018] noted that the impact of the thermodynamics is fairly well
74 understood from the basic physics, whereas the part played by the atmospheric dynamics
75 is much more complex and ambiguous. Therefore, this study aims to understand the phys-

76 ical mechanisms which cause summer EE heatwaves – specifically focusing on the AMM
77 – using a combination of observational data and climate model perturbation experiments.

78 Here, using observations and climate model experiments, we aim to understand the in-
79 fluence of a teleconnection pattern – which is associated with the AMM– on the heatwaves
80 over the EE region (50°E – 70°E and 45°N – 60°N ; Figure 1) during boreal summer (June-
81 August). The AMM, which results from the coupled ocean and atmospheric variability over
82 the Atlantic basin [75°E – 15°W , 21°S – 32°N], triggers a persistent planetary-scale Rossby
83 wave train in the upper-levels of the atmosphere in the northern hemisphere. This wave
84 train features anticyclonic circulation/blocking patterns leading to an increased tempera-
85 ture over the EE region. Further, with the use of climate model perturbation experiments
86 and control simulations (detailed in the section below), we investigate the underlying mech-
87 anism through which the AMM modulates the EE summer heatwaves. In addition, we
88 show that the influence of AMM on EE temperature is independent of the other promi-
89 nent teleconnection patterns on inter-annual timescales, such as the El Niño-Southern
90 Oscillation (ENSO) and NAO, among other well-established drivers of mid-latitudinal cli-
91 mate. Finally, we demonstrate that, along with other dominant climate modes, AMM can
92 significantly improve the predictability of EE summer temperature.

93 **2. Data and Methods**

94 The assessment of temperature characteristics during summer over EE from 1980–
95 2019 is performed using the fifth generation ECMWF atmospheric reanalysis (ERA5)
96 data [Hersbach et al., 2020] as it is capable enough to capture observed temperature

97 variability and extremes over the region of interest [Velikou et al., 2022]. SST data is
98 obtained from the sea ice and sea surface temperature reconstruction (HadISST), produced
99 by the Met Office Hadley Centre [Rayner et al., 2003]. Monthly estimates of the AMM
100 index are obtained from the NOAA Earth System Research Library, available at [https://](https://www.esrl.noaa.gov/psd/data/timeseries/monthly/AMM/)
101 www.esrl.noaa.gov/psd/data/timeseries/monthly/AMM/ for the period 1948–present.

102 The large-scale atmospheric variables such as geopotential height and winds at different
103 pressure levels are obtained from the National Centers for Environmental Prediction-
104 National Center for Atmospheric Research (NCEP–NCAR) reanalysis [Kalnay et al., 1996].

105 The AMM is the leading mode of coupled atmospheric and ocean variability in the
106 Atlantic Ocean basin [Chiang and Vimont, 2004]. It can be estimated by applying the
107 maximum covariance analysis (MCA) to the tropical Atlantic basin, assessing the co-
108 variability of SSTs and 10m surface winds. It is worth mentioning that while estimating
109 the AMM index, the effect of the El Nino Southern Oscillation (ENSO) is removed [Chiang
110 and Vimont, 2004]. The positive feedback between surface winds, evaporation, and SST
111 – the wind-evaporation-SST (WES) feedback – is the main cause of the meridional modes
112 [Xie et al., 2005; Chiang and Vimont, 2004]. AMM is an important driver of the climate
113 variability in several regions e.g., the Indian monsoon [Vittal et al., 2020a], western North
114 Pacific tropical cyclones [Zhang et al., 2017], and Atlantic tropical cyclones [Vimont and
115 Kossin, 2007; Patricola et al., 2014]. Nonetheless, knowledge of the influence of AMM on
116 European summer climatology is limited and as such disentangling their role along with
117 other prominent climate modes (NAO, ENSO) is the main focus of this study.

118 Given the strong influence exerted by the ENSO on the surrounding areas, particularly

119 over the Atlantic Ocean , we therefore try to isolate the ENSO signal. The ENSO signal
 120 here is removed by calculating the residual time series [Kucharski et al., 2009]:

$$SST_R(t) = SST(t) - SST_{ENSO}(t) \quad (1)$$

121 where

$$SST_{ENSO}(t) = b NINO34(t) \quad (2)$$

122 where b is calculated using the linear regression between SST at a respective grid and
 123 Niño3.4 index.

124 The wave activity flux (WAF) is implemented to understand the energy propagation
 125 pathways originating from the AMM and their influence on EE heatwaves. It is considered
 126 as a diagnostic tool for highlighting the propagation, source and sink of a packet of sta-
 127 tionary or migratory quasi-geostrophic wave [Takaya and Nakamura, 2001]. It is usually
 128 estimated using information at 250 hPa pressure level, following the expression equation
 129 [Takaya and Nakamura, 2001]:

$$W = \frac{p \cos \varphi}{2|\mathbf{U}|} \left(\begin{array}{l} \frac{U}{a^2 \cos^2 \varphi} \left[\left(\frac{\partial \psi'}{\partial \lambda} \right)^2 - \psi' \left(\frac{\partial^2 \psi'}{\partial \lambda^2} \right) \right] + \frac{V}{a^2 \cos \varphi} \left[\frac{\partial \psi'}{\partial \lambda} \frac{\partial \psi'}{\partial \varphi} - \psi' \frac{\partial^2 \psi'}{\partial \lambda \partial \varphi} \right] \\ \frac{U}{a^2 \cos \varphi} \left[\frac{\partial \psi'}{\partial \lambda} \frac{\partial \psi'}{\partial \varphi} - \psi' \frac{\partial^2 \psi'}{\partial \lambda \partial \varphi} \right] + \frac{V}{a^2} \left[\left(\frac{\partial \psi'}{\partial \varphi} \right)^2 - \psi' \left(\frac{\partial^2 \psi'}{\partial \varphi^2} \right) \right] \\ \frac{f_0^2}{N^2} \left\{ \frac{U}{a \cos \varphi} \left[\frac{\partial \psi'}{\partial \lambda} \frac{\partial \psi'}{\partial z} - \psi' \frac{\partial^2 \psi'}{\partial \lambda \partial z} \right] + \frac{V}{a} \left[\frac{\partial \psi'}{\partial \varphi} \frac{\partial \psi'}{\partial z} - \psi' \frac{\partial^2 \psi'}{\partial \varphi \partial z} \right] \right\} \end{array} \right) \quad (3)$$

130 where W denotes the WAF, p is pressure, ψ is the streamfunction, $\mathbf{U} = (U, V)$ is
 131 horizontal wind vector, with U and V denoting the zonal and meridional wind components,

132 respectively; λ and φ are longitude and latitude, respectively; f_0 is the Coriolis parameter;
133 N is the Brunt-Vaisala frequency; a is Earth’s radius and the prime represents the anomaly
134 with respect to the climatological mean from 1951–2019.

135 *2.1. Climate model perturbation experiment*

136 To ascertain the role of the tropical Atlantic Ocean SST variability and the EE region
137 heatwaves and the associated large-scale circulation, we perform a climate model pertur-
138 bation experiment which is integrated over 25 years. Here, we use the atmospheric general
139 circulation model developed by the International Centre for Theoretical Physics (ICTP
140 AGCM) [Molteni, 2003; Kucharski et al., 2013], following the two sets of complementary
141 simulations. The first set of the simulation considers prescribing the seasonal climatol-
142 ogy of SST based on ECMWF reanalysis (CLIM; averaged from 1979 to 2008). Next, in
143 the second simulation, to evaluate the response of EE heatwaves, the observed composite
144 anomaly of SST during the positive phase of AMM over the AMM region for the sum-
145 mer season (June–August) is superimposed on the monthly climatology, keeping the SST
146 identical to the CLIM simulation for other months. The subtraction of the CLIM simu-
147 lation with the SST anomaly-forced simulation then provides the response of large-scale
148 atmospheric circulation to the AMM.

149 *2.2. Control climate model experiment*

150 In addition to the observational/reanalysis data that we use to understand the associa-
151 tion between AMM and EE heatwaves, we also use a fully-coupled long-term Geophysical
152 Fluid Dynamics Laboratory (GFDL) Forecast-Oriented Low Ocean Resolution (FLOR)

153 coupled climate model control experiments [Vecchi et al., 2014; Zhang et al., 2016; Hari
154 et al., 2022]. The radiative forcing and land use are specified at 1860 levels and thus
155 referred to as pre-industrial experiments. The atmosphere and land components of FLOR
156 have the horizontal resolution of $\simeq 0.5^\circ$ with 32 vertical levels. FLOR has an updated pa-
157 rameterization for mesoscale eddies and a parameterization for submesoscale mixed layer
158 eddies [Wittenberg et al., 2018]. Moreover, this model has an enhanced capability in cap-
159 turing the near-surface equatorial upwelling compared to their predecessors. A detailed
160 information regarding the GFDL FLOR model is reported in Vecchi et al [Vecchi et al.,
161 2014]. We use these simulations to test if the established relation between AMM-EE
162 heatwave variability also occurs in the GFDL-FLOR long-term control simulations, which
163 would impart a dynamical framework – mainly to understand the causation of this rela-
164 tionship [Zhang et al., 2016]. The control experiments are performed for a total of 2500
165 years, however, here we focus on 300 years – later part of the first 1000 years – to analyse
166 AMM and EE heatwaves. The AMM index in this experiment is estimated – as proposed
167 by [Chiang and Vimont, 2004] – through the MCA approach based on the corresponding
168 SSTs and surface wind fields.

169 For the estimation of the AMM index, we first remove the seasonal cycle from monthly
170 fields, detrend both the SST and wind data and then apply a three-month running mean
171 for both variables. Further, to remove the influence of ENSO on both SST and winds (refer
172 Eq. 1 and 2), we remove the equatorial Pacific Cold Tongue (SST averaged over 180°W –
173 90°W , 6°S – 6°N) from all the grid points for both the variables [Chiang and Vimont, 2004].
174 Once this pre-processing is done, we finally apply the MCA by formulating the covariance

175 matrix between SST and surface winds. This matrix is decomposed through Singular
176 Value Decomposition (SVD). The leading statistical mode from this decomposition forms
177 an AMM index for the model [Chiang and Vimont, 2004].

178 *2.3. Statistical PCMCI causal analysis*

179 To complement the above analysis of the climate model experiments – linking AMM
180 to EE heatwaves – we further perform a robust statistical causal analysis based on Peter
181 and Clark momentary conditional independence (PCMCI) algorithm [Runge et al., 2019].
182 The PCMCI is a two-step algorithm, wherein in the first step, the relevant conditions for
183 each considered variable (both, EE temperature and other climatic modes) are identified
184 by iterative independence testing. The second step, however, is to test the link between
185 the two variables is causal. Here, to correct the unreasonable p-values – due to multiple
186 significance testing Di Capua et al. [2020] – a false discovery rate approach [Benjamini and
187 Hochberg, 1995] is implemented. A detailed methodology underlying the PCMI method
188 is provided by Runge et al. [2019] and Di Capua et al. [2020]. Here along with AMM,
189 we also consider North Atlantic Oscillation (NAO, Wunsch [1999]), El Niño–Southern
190 Oscillation (ENSO, Schneidereit et al. [2012]) and Arctic Amplification (AA Cohen et al.
191 [2014]). The AA is measured as the change in surface air temperature over the Arctic
192 (70°N – 90°N) relative to mid-latitudes (30°N – 60°N ; Ionita et al. [2020]). We selected these
193 climate modes because of their controls on the European climate variability – specifically
194 during the summer season [Sun et al., 2016; Cohen et al., 2014].

195 **3. Results and Discussion**

196 *3.1. Observational analysis*

197 We start our analysis by exploring the 2010 Eastern European (EE) heatwave event –
198 which is one of the hottest events ever recorded in the region [Rasmijn et al., 2018] – and
199 the large-scale air-sea interaction patterns, including SST and near-surface wind anoma-
200 lies corresponding to this event. It is evident from Figure 1 that temperature anomalies
201 during the summer of 2010 over Europe – specifically over EE – were substantially warmer
202 than usual (> 2 °C higher compared to the respective climatology over the EE region).
203 It is reported that this particular event shattered heatwave records both in terms of the
204 intensity and the impacts [Barriopedro et al., 2011] and demonstrated the societal vulner-
205 ability to such persistent extreme weather [Rasmijn et al., 2018]. Thus, understanding the
206 physical mechanism responsible for such persistent events forms an important step towards
207 climate adaptation, as much as it is in investigating the impacts of global warming on the
208 occurrence and severity of these extreme temperature events [Marotzke et al., 2017].

209 We extend the analysis beyond the 2010 event and observe that there are several
210 hot summers over the EE region in the historical record – based on spatially averaged
211 temperature over the EE region during summer (June-August). However, the 2010 event
212 was exceptional in terms of intensity (Figure 1b). We proceed to analyse the large-scale air-
213 sea interaction patterns during these warm summers (Figure 1c) and notice a predominant
214 pattern of positive SST anomalies over the northern part of the tropical Atlantic region and
215 negative anomalies in the southern part – with the influence of ENSO is removed (refer Eq.

216 1 and 2). This pattern resembles strongly the spatial pattern of the Atlantic Meridional
217 Mode (AMM) [Chiang and Vimont, 2004] (rectangular box; 75°E–15°W, 21°S–32°N; in
218 Fig. 1c) or the northern tropical Atlantic (NTA) mode [Chen et al., 2015]. The spatial
219 patterns of these two modes, i.e., AMM and NTA, are exactly similar; their correlation is
220 0.86. The wind patterns i.e., movement from the cooler region to the warmer ones over
221 the tropical Atlantic – further corroborate the prominence of AMM [Chiang and Vimont,
222 2004] during the warmer summers over the EE region.

223 To uncover the association of AMM with the inter-annual variability of summer tem-
224 perature across the EE region, we relate the observed summer temperature anomalies with
225 the AMM index over the period 1980-2019. A dipole behaviour is noticed over the Euro-
226 pean region (Figure 1d) – with the majority of the Central and Northern European region
227 having a negative association and the Eastern region having a positive association of their
228 respective temperature anomalies with AMM index. Moreover, the strongest signal is
229 apparent over the EE region (Figure 1d), with temperature anomalies being significantly
230 warmer during the 2010 summer (Figure 1a). Similar results were obtained when we per-
231 formed the analysis over a longer duration (1951 – 2019) using the NCEP-NCAR reanalysis
232 temperature dataset (not shown here). Overall, this indicates that a strong positive phase
233 of AMM may enforce the prominent warmer conditions over EE – also corroborated with
234 the composite analysis results from the winds and SSTs patterns over the AMM region
235 (Figure 1c). Significant differences in the EE temperature are observed between the years
236 with the strong positive and negative phases of AMM (Figure 1e; mean difference of 0.9°C
237 with p-value < 0.1 based on a non-parametric bootstrap sampling technique [Wilks, 2011;

238 Hari et al., 2022]).

239 The above analysis shows a significant positive association of the EE summer temper-
240 ature with the AMM index. Next, we investigate underlying large-scale processes through
241 which the AMM could be possibly linked to the EE summer temperature variability. We
242 start by examining the 500 hPa geopotential height patterns – as the AMM is reported
243 to cause changes in the tropospheric circulation [Zhang et al., 2017; Vittal et al., 2020a].
244 Figure 2a shows the association of 500 hPa geopotential height with the summer AMM
245 index over the period 1951 – 2019. Apparent is the higher geopotential height with a
246 prominent anticyclonic circulation over the EE region. This synoptic situation reduces
247 the advection of warm air away from the region, and simultaneously reduces cloudiness,
248 which further intensifies the heatwave conditions [Rasmijn et al., 2018]. In addition, the
249 favourable conditions for a blocking high can lead to a persistent flow pattern Chatterjee
250 et al. [2021] in response to the positive phase of the AMM (Figure 2b). Disturbance of SST
251 anomalies over the tropical Atlantic region and their linkage to stationary Rossby wave
252 trains – which propagate eastward and poleward – have also been identified in previous
253 studies [Li et al., 2014, 2015, 2016; Ren et al., 2022].

254 The AMM usually shifts the inter-tropical convergence zone towards the anomalously
255 warmer region over the tropical Atlantic basin, through a shift in deep convection [Chiang
256 and Vimont, 2004]. This further increases rainfall over the warmer region of the tropi-
257 cal Atlantic Ocean[Foltz et al., 2012]. Accompanying with the convection process is an
258 anomalous divergence of the atmospheric flow at the planetary scale [Jin and Hoskins,
259 1995]. When this divergence coincides with a favourable background vorticity gradient,

260 the Rossby waves are generated [Sardeshmukh and Hoskins, 1988; Luo et al., 2019; Rudeva
261 and Simmonds, 2021]. We can see a Rossby wave train propagating eastward from the
262 Atlantic basin to the EE region during the positive phase of AMM (Figure 2c). Along with
263 the Rossby wave train pathway, we notice an association with the eddy streamfunctions
264 patterns (Figure 2c; represented with the shading) which greatly resembles the geopotential
265 height patterns as observed in Figure 2a. Further, we observe an alternate positive and
266 negative Rossby wave sources along the atmospheric wave train (Figure 3a). The largest
267 negative Rossby wave source is found over the tropical Atlantic around 10° – 20° N (Figure
268 3a) where strong upward motion located (Figure 3b) and large positive precipitation
269 (Figure 3c) are noticed. Thus with positive precipitation and upward motion (Figure 3b-c)
270 play a crucial role in the formation of the strong negative Rossby wave source over the
271 tropical Atlantic (Figure 3a) – which indicates the atmospheric wave originating from the
272 tropical Atlantic [Chen et al., 2020, 2021]. Overall, these observational analyses reveal
273 a possible mechanism through which the AMM can affect the inter-annual variability of
274 summer temperatures over the EE region. The positive phase of AMM during summer –
275 induced via the deep convection process – causes an eastward propagation of the Rossby
276 wave train which triggers a blocking high over the EE region leading to hotter conditions
277 with positive temperature anomalies over the region.

278 *3.2. Climate model control and perturbation analysis*

279 To further ascertain the above findings and moving from the correlation/regression
280 analysis to causation, we next performed a controlled climate model perturbation exper-

281 iment with the ICTP AGCM model [Molteni, 2003; Kucharski et al., 2013; Vittal et al.,
282 2020b]. Results of the perturbation experiment are in good accord with the AMM-EE
283 response noted above in the observational analysis (Figure 4a). As with the observations,
284 here also, we find an increased geopotential height with a prominent anticyclonic circula-
285 tion over the EE region, which further causes an increased temperature over the EE region
286 (Figure 4b). Moreover, in this case, we observe high and low centres of geopotential height
287 mimicking a Rossby wave-like pattern – similar to the observations. Additionally, we see
288 the eastward Rossby wave train propagation from the Atlantic basin to the EE region
289 during the positive phase of AMM (Figure 4c and d). The eddy streamfunction patterns
290 also resemble the results of observational analysis quite well (Figure 4d), and thereby
291 supporting the possible role of AMM in the eastward propagation of the Rossby wave.

292 Here, using this long-term control experiment, we complement the observational and
293 perturbation analysis results – under control conditions of radiative forcings and landuse
294 configurations (Vecchi et al. [2014]). The reason for using this is to test if the established
295 relation between AMM-EE summer temperature variability is robust given the long-term
296 climate simulations under the fixed boundary conditions. This further assists in providing
297 a mechanistic framework to understand the causation of the AMM vs. EE temperature
298 relationship [Zhang et al., 2016; Hari et al., 2022]. The long-term control simulation
299 could able to represent the meridional pattern reasonably well (Figure 5a). Further, we
300 also find that the long-term control simulations are in good accord with the AMM-EE
301 response as observed before in both observational and climate perturbation experiment
302 results (Figure 5b). As with the observational analysis, here also, we find an increased

303 geopotential height with a prominent anticyclonic circulation over the EE region during
304 the positive phase of the AMM. This further causes an increased temperature anomaly
305 over the EE region (Figure 5c). Although we notice an overall similarity between observed
306 and modelled responses to AMM, we do notice some biases in the model, which among
307 other things could be due to imprints of anthropogenic warming conditions [Differbaugh
308 et al., 2015; Williams et al., 2020; Bonfils et al., 2020; Dai, 2013] in observational datasets,
309 inability to represent key ocean/atmosphere feedback [Peings and Magnusdottir, 2015],
310 differences in spatial resolutions and, more importantly, the different forcing conditions.

311 *3.3. Causal analysis*

312 The aforementioned analysis establishes a relationship with a potential linkage between
313 the AMM and the summer EE temperature variability. Herein, we further extend our
314 research to understand the implications of this established linkage to the predictability of
315 EE temperature, considering other important large-scale climatic modes – such as ENSO,
316 NAO and AA along with AMM during the summer months. The ENSO is related to the
317 EE climate by forcing an eastward propagation of Rossby wave reaching the EE region [Sun
318 et al., 2016] – resembles the pattern partly during the positive phase of AMM. However, the
319 partial correlation analysis results suggest a persistent relationship between AMM and EE
320 temperature even while accounting for the effect of ENSO (Figure 6a). This relationship
321 (AMM vs. EE temperature) was robust even in the presence of other important climatic
322 modes such as NAO and AA (Figure 6a). To further strengthen the evidence of this
323 robustness, we carry out a detailed statistical causal analysis using the PCMCI causal

324 discovery framework [Runge et al., 2019]. Results of the PCMCI analysis confirm that the
325 AMM positively drives the EE summer temperature variability (Figure 6c) – in line with
326 the above results. As with some of the previous studies [Trenberth and Fasullo, 2012;
327 Sun et al., 2016], we also notice that the ENSO and NAO negatively influence the EE
328 temperature variability, and AA does not have a casual relationship with the inter-annual
329 variability of EE temperature (Figure 6c). Moreover, the important aspect here is that
330 AMM, ENSO and NAO are influencing the EE temperature variability (Figure 6b) in
331 a mutually exclusive and independent way – in line with the partial correlation analysis
332 (Figure 5a).

333 4. Conclusions

334 Heatwaves are predicted to increase both in their frequency and intensity in the future
335 along with an increase in the global mean temperature – over the northern Hemisphere
336 [Barriopedro et al., 2011], and Europe in particular [Rasmijn et al., 2018]. Nonetheless,
337 for proper mitigation and adaptation strategies, policy-makers would need a reliable pre-
338 diction of these hydroclimatic extremes and for this, the information pertaining to the
339 causation of such events is important [Bellprat et al., 2019]. To this end, there have been
340 many studies exist to understand the physical mechanism responsible for such events over
341 the EE region. However, the role of tropical Atlantic ocean on the EE temperature vari-
342 ability is not well addressed – specifically the influence of AMM, one of the dominant
343 climatic modes in the tropical Atlantic Ocean, on the EE temperature variability. To this
344 end, we have investigated the role of the AMM on the EE summer temperature variability

345 – the consistency and the robustness of which are confirmed both by the observations and
346 climate model perturbation experiments as well with robust (causal) statistical methods.
347 The mechanism with which it influences the EE region temperature variability is through
348 the eastward propagation of Rossby wave trains – which, in turn, cause an anomalous
349 anticyclonic circulation over the region and lead to higher anomalous temperature over
350 the EE region.

351 Previous studies do show that the EE summer temperature variability are influenced by
352 some of the important large-scale climatic modes – such as ENSO [Brönnimann, 2007; Sun
353 et al., 2016] and NAO [Hurrell, 1995; Krüger et al., 2020; Bierkens and Van Beek, 2009; Li
354 et al., 2020]. In this study, we found that both these climatic modes, along with the AMM
355 do play an important role in explaining the temperature variability over EE (Figure 6b).
356 The relative importance analysis further reveals that the primary climatic mode – ENSO
357 – has the highest importance, followed by AMM and NAO. However, all these climatic
358 modes have a significant influence on the EE temperature variability and moreover, they
359 are mutually exclusive in explaining the variability – as seen in the causal analysis (Figure
360 6c). It is also observed that these climatic modes have a significant relation with EE
361 temperature variability only during the summer. However, the preceding winter months
362 of ENSO and NAO do show a significant association with the summer AMM (Figure
363 6c). A study by López-Parages and Terray [2022] specifically mentioned that ENSO –
364 one of its most robust remote impacts is that they affect the tropical Atlantic SST, i.e.,
365 AMM, especially during the preceding months to summer. The telecommunication can
366 be explained through different mechanisms, such as (i) Rossby wave trains propagation

367 [Enfield and Mayer, 1997], (ii) changes in the zonal (Walker) and meridional (Hadley)
368 cells [Wang, 2004] and and (iii) a secondary Gill-type structure in the tropical Atlantic
369 [Doblas-Reyes et al., 2017]. Nonetheless, we believe a complete understanding of these
370 aspects is beyond the scope of the present study and can be considered a potential future
371 research. In summary, our results add to previous efforts in associating the EE temperature
372 variability to large-scale climate modes reliably and thereby provide a pathway to predict
373 such extreme events more accurately.

374 **Acknowledgements**

375 VH acknowledges support from the Faculty Research Scheme of IIT (ISM) Dhanbad
376 (FRS(176)/2022-2023/ESE). RK and OR acknowledges support from the bilateral project
377 XEROS (eXtreme EuRopean drOughtS: multimodel synthesis of past, present and future
378 events), funded by the Deutsche Forschungsgemeinschaft (grant RA 3235/1-1) and Czech
379 Science Foundation (grant 19-24089J). MC was supported by NERC NE/S004645/1. AK
380 acknowledges support from the European Union Horizon 2020 Programme (DOWN2EARTH,
381 869550). The authors also acknowledge efforts of different organizations/people for making
382 the data available for this work which include ERA5, NCEP-NCAR reanalysis and GFDL-
383 FLOR control simulation datasets. We also thank Dr. Fred Kucharski for providing access
384 to the ICTP AGCM model.

385 **Data Availability**

386 Data used here – temperature and large-scale atmospheric variables – can be down-
387 loaded from: ERA5 (<https://www.ecmwf.int/en/forecasts/datasets/reanalysis-datasets/era5>), NCEP-NCAR reanalysis data (<https://psl.noaa.gov/data/gridded/data.ncep.reanalysis.html>). The climate indicators used in the present study can be procured
389 from: AMM (<https://www.esrl.noaa.gov/psd/data/timeseries/monthly/AMM/>), NAO
390 (<https://www.cpc.ncep.noaa.gov/data/teledoc/nao.shtml>) and ENSO (https://origin.cpc.ncep.noaa.gov/products/analysis_monitoring/ensostuff/ONI_v5.php).
392

393 **References**

394 Alexander, L., 2011. Extreme heat rooted in dry soils. *Nature Geoscience* 4, 12–13.

395 Barriopedro, D., Fischer, E.M., Luterbacher, J., Trigo, R.M., García-Herrera, R., 2011.
396 The hot summer of 2010: redrawing the temperature record map of Europe. *Science*
397 332, 220–224.

398 Bellprat, O., Guemas, V., Doblas-Reyes, F., Donat, M.G., 2019. Towards reliable extreme
399 weather and climate event attribution. *Nature Communications* 10, 1–7.

400 Benjamini, Y., Hochberg, Y., 1995. Controlling the false discovery rate: a practical and
401 powerful approach to multiple testing. *Journal of the Royal Statistical Society: Series B*
402 (Methodological) 57, 289–300.

403 Bierkens, M., Van Beek, L., 2009. Seasonal predictability of European discharge: NAO
404 and hydrological response time. *Journal of Hydrometeorology* 10, 953–968.

405 Bonfils, C.J.W., Santer, B.D., Fyfe, J.C., Marvel, K., Phillips, T.J., Zimmerman, S.R.H.,
406 2020. Human influence on joint changes in temperature, rainfall and continental aridity.
407 *Nat. Clim. Change* 10, 726–731. doi:10.1038/s41558-020-0821-1.

408 Brönnimann, S., 2007. Impact of El Niño–Southern Oscillation on European climate. *Reviews*
409 *of Geophysics* 45.

410 Brunner, L., Schaller, N., Anstey, J., Sillmann, J., Steiner, A.K., 2018. Dependence

411 of present and future european temperature extremes on the location of atmospheric
412 blocking. *Geophysical research letters* 45, 6311–6320.

413 Cassou, C., Terray, L., Phillips, A.S., 2005. Tropical atlantic influence on european heat
414 waves. *Journal of climate* 18, 2805–2811.

415 Chatterjee, S., Ravichandran, M., Murukesh, N., Raj, R.P., Johannessen, O.M., 2021. A
416 possible relation between arctic sea ice and late season indian summer monsoon rainfall
417 extremes. *npj Climate and Atmospheric Science* 4, 1–6.

418 Chen, S., Wu, R., Chen, W., 2015. The changing relationship between interannual vari-
419 ations of the north atlantic oscillation and northern tropical atlantic sst. *Journal of*
420 *Climate* 28, 485–504.

421 Chen, S., Wu, R., Chen, W., 2021. Influence of north atlantic sea surface temperature
422 anomalies on springtime surface air temperature variation over eurasia in cmip5 models.
423 *Climate Dynamics* 57, 2669–2686.

424 Chen, S., Wu, R., Chen, W., Hu, K., Yu, B., 2020. Structure and dynamics of a springtime
425 atmospheric wave train over the north atlantic and eurasia. *Climate Dynamics* 54, 5111–
426 5126.

427 Chen, S., Wu, R., Song, L., Chen, W., 2019. Interannual variability of surface air temper-
428 ature over mid-high latitudes of eurasia during boreal autumn. *Climate Dynamics* 53,
429 1805–1821.

430 Chiang, J.C., Vimont, D.J., 2004. Analogous Pacific and Atlantic meridional modes of
431 tropical atmosphere–ocean variability. *Journal of Climate* 17, 4143–4158.

432 Cohen, J., Screen, J.A., Furtado, J.C., Barlow, M., Whittleston, D., Coumou, D., Francis,
433 J., Dethloff, K., Entekhabi, D., Overland, J., et al., 2014. Recent Arctic amplification
434 and extreme mid-latitude weather. *Nature geoscience* 7, 627–637.

435 Dai, A., 2013. Increasing drought under global warming in observations and models. *Nat.*
436 *Clim. Change* 3, 52–58. doi:10.1038/nclimate1633.

437 Della-Marta, P.M., Luterbacher, J., von Weissenfluh, H., Xoplaki, E., Brunet, M., Wanner,
438 H., 2007. Summer heat waves over western europe 1880–2003, their relationship to large-
439 scale forcings and predictability. *Climate Dynamics* 29, 251–275.

440 Di Capua, G., Kretschmer, M., Donner, R.V., Van Den Hurk, B., Vellore, R., Krishnan,
441 R., Coumou, D., 2020. Tropical and mid-latitude teleconnections interacting with the
442 indian summer monsoon rainfall: a theory-guided causal effect network approach. *Earth*
443 *System Dynamics* 11, 17–34.

444 Di Capua, G., Sparrow, S., Kornhuber, K., Rousi, E., Osprey, S., Wallom, D., van den
445 Hurk, B., Coumou, D., 2021. Drivers behind the summer 2010 wave train leading to
446 russian heatwave and pakistan flooding. *npj Climate and Atmospheric Science* 4, 1–14.

447 Diffenbaugh, N.S., Swain, D.L., Touma, D., 2015. Anthropogenic warming has increased
448 drought risk in California. *Proc. Natl. Acad. Sci. U.S.A.* 112, 3931–3936. doi:10.1073/
449 *pnas.1422385112*.

450 Doblas-Reyes, F.J., García-Serrano, J., Cassou, C., Douville, H., Giannini, A., 2017. Re-
451 visiting the enso teleconnection to the tropical north atlantic. *Journal of Climate* 30.

452 Dole, R., Hoerling, M., Perlwitz, J., Eischeid, J., Pegion, P., Zhang, T., Quan, X.W., Xu,
453 T., Murray, D., 2011. Was there a basis for anticipating the 2010 russian heat wave?
454 *Geophysical Research Letters* 38.

455 Earl, N., Simmonds, I., 2018. Spatial and temporal variability and trends in 2001–2016
456 global fire activity. *Journal of Geophysical Research: Atmospheres* 123, 2524–2536.

457 Enfield, D.B., Mayer, D.A., 1997. Tropical atlantic sea surface temperature variability and
458 its relation to el niño-southern oscillation. *Journal of Geophysical Research: Oceans* 102,
459 929–945.

460 Fischer, E.M., Seneviratne, S.I., Lüthi, D., Schär, C., 2007. Contribution of land-
461 atmosphere coupling to recent european summer heat waves. *Geophysical Research*
462 *Letters* 34.

463 Folland, C.K., Knight, J., Linderholm, H.W., Fereday, D., Ineson, S., Hurrell, J.W., 2009.
464 The summer north atlantic oscillation: past, present, and future. *Journal of Climate*
465 22, 1082–1103.

466 Foltz, G.R., McPhaden, M.J., Lumpkin, R., 2012. A strong atlantic meridional mode
467 event in 2009: The role of mixed layer dynamics. *Journal of Climate* 25, 363–380.

468 García-Herrera, R., Díaz, J., Trigo, R.M., Luterbacher, J., Fischer, E.M., 2010. A review

469 of the european summer heat wave of 2003. *Critical Reviews in Environmental Science*
470 *and Technology* 40, 267–306.

471 Hari, V., Ghosh, S., Zhang, W., Kumar, R., 2022. Strong influence of north pacific ocean
472 variability on indian summer heatwaves. *Nature communications* 13, 1–11.

473 Hersbach, H., Bell, B., Berrisford, P., Hirahara, S., Horányi, A., Muñoz-Sabater, J., Nico-
474 las, J., Peubey, C., Radu, R., Schepers, D., et al., 2020. The era5 global reanalysis.
475 *Quarterly Journal of the Royal Meteorological Society* 146, 1999–2049.

476 Hurrell, J.W., 1995. Decadal trends in the North Atlantic Oscillation: regional tempera-
477 tures and precipitation. *Science* 269, 676–679.

478 Ionita, M., Nagavciuc, V., Kumar, R., Rakovec, O., 2020. On the curious case of the
479 recent decade, mid-spring precipitation deficit in central Europe. *npj Clim Atmos Sci*
480 3, 1–10.

481 Jin, F., Hoskins, B.J., 1995. The direct response to tropical heating in a baroclinic atmo-
482 sphere. *Journal of the atmospheric sciences* 52, 307–319.

483 Kalnay, E., Kanamitsu, M., Kistler, R., Collins, W., Deaven, D., Gandin, L., Iredell, M.,
484 Saha, S., White, G., Woollen, J., Zhu, Y., Chelliah, M., Ebisuzaki, W., Higgins, W.,
485 Janowiak, J., Mo, K.C., Ropelewski, C., Wang, J., Leetmaa, A., Reynolds, R., Jenne, R.,
486 Joseph, D., 1996. The NCEP/NCAR 40-Year Reanalysis Project. *Bull. Am. Meteorol.*
487 *Soc.* 77, 437–472. doi:10.1175/1520-0477(1996)077<0437:TNYRP>2.0.CO;2.

488 Kautz, L.A., Martius, O., Pfahl, S., Pinto, J.G., Ramos, A.M., Sousa, P.M., Woollings,
489 T., 2022. Atmospheric blocking and weather extremes over the euro-atlantic sector—a
490 review. *Weather and Climate Dynamics* 3, 305–336.

491 Krüger, J., Pilch Kedzierski, R., Bunke, K., Matthes, K., 2020. Impact of cold north
492 atlantic sst and jet stream anomalies on european heat waves, in: AGU Fall Meeting
493 Abstracts, pp. A246–01.

494 Kucharski, F., Bracco, A., Yoo, J., Tompkins, A., Feudale, L., Ruti, P., Dell’Aquila, A.,
495 2009. A gill–matsuno-type mechanism explains the tropical atlantic influence on african
496 and indian monsoon rainfall. *Quarterly Journal of the Royal Meteorological Society:*
497 *A journal of the atmospheric sciences, applied meteorology and physical oceanography*
498 135, 569–579.

499 Kucharski, F., Molteni, F., King, M.P., Farneti, R., Kang, I.S., Feudale, L., 2013. On
500 the need of intermediate complexity general circulation models: A “speedy” example.
501 *Bulletin of the American Meteorological Society* 94, 25–30.

502 Lhotka, O., Kyselý, J., Plavcová, E., 2018. Evaluation of major heat waves’ mechanisms
503 in euro-cordex rcms over central europe. *Climate dynamics* 50, 4249–4262.

504 Li, M., Yao, Y., Simmonds, I., Luo, D., Zhong, L., Chen, X., 2020. Collaborative impact
505 of the nao and atmospheric blocking on european heatwaves, with a focus on the hot
506 summer of 2018. *Environmental Research Letters* 15, 114003.

507 Li, X., Holland, D.M., Gerber, E.P., Yoo, C., 2014. Impacts of the north and tropical
508 atlantic ocean on the antarctic peninsula and sea ice. *Nature* 505, 538–542.

509 Li, X., Holland, D.M., Gerber, E.P., Yoo, C., 2015. Rossby waves mediate impacts of
510 tropical oceans on west antarctic atmospheric circulation in austral winter. *Journal of*
511 *Climate* 28, 8151–8164.

512 Li, X., Xie, S.P., Gille, S.T., Yoo, C., 2016. Atlantic-induced pan-tropical climate change
513 over the past three decades. *Nature Climate Change* 6, 275–279.

514 Liu, X., He, B., Guo, L., Huang, L., Chen, D., 2020. Similarities and differences in the
515 mechanisms causing the european summer heatwaves in 2003, 2010, and 2018. *Earth’s*
516 *Future* 8, e2019EF001386.

517 López-Parages, J., Terray, L., 2022. Tropical north atlantic response to enso: sensitivity
518 to model spatial resolution. *Journal of Climate* 35, 3–16.

519 Luo, D., Chen, X., Overland, J., Simmonds, I., Wu, Y., Zhang, P., 2019. Weakened
520 potential vorticity barrier linked to recent winter arctic sea ice loss and midlatitude cold
521 extremes. *Journal of Climate* 32, 4235–4261.

522 Marotzke, J., Jakob, C., Bony, S., Dirmeyer, P.A., O’Gorman, P.A., Hawkins, E., Perkins-
523 Kirkpatrick, S., Quéré, C.L., Nowicki, S., Paulavets, K., et al., 2017. Climate research
524 must sharpen its view. *Nature climate change* 7, 89–91.

525 Meehl, G.A., Tebaldi, C., 2004. More intense, more frequent, and longer lasting heat
526 waves in the 21st century. *Science* 305, 994–997.

- 527 Miralles, D.G., Gentile, P., Seneviratne, S.I., Teuling, A.J., 2019. Land–atmospheric
528 feedbacks during droughts and heatwaves: state of the science and current challenges.
529 *Annals of the New York Academy of Sciences* 1436, 19–35.
- 530 Miralles, D.G., Teuling, A.J., Van Heerwaarden, C.C., Vilà-Guerau de Arellano, J., 2014.
531 Mega-heatwave temperatures due to combined soil desiccation and atmospheric heat
532 accumulation. *Nature geoscience* 7, 345–349.
- 533 Molteni, F., 2003. Atmospheric simulations using a gcm with simplified physical
534 parametrizations. i: Model climatology and variability in multi-decadal experiments.
535 *Climate Dynamics* 20, 175–191.
- 536 Otto, F.E., Massey, N., van Oldenborgh, G.J., Jones, R.G., Allen, M.R., 2012. Reconciling
537 two approaches to attribution of the 2010 russian heat wave. *Geophysical Research*
538 *Letters* 39.
- 539 Patricola, C.M., Saravanan, R., Chang, P., 2014. The impact of the el niño–southern
540 oscillation and atlantic meridional mode on seasonal atlantic tropical cyclone activity.
541 *Journal of Climate* 27, 5311–5328.
- 542 Peings, Y., Magnusdottir, G., 2015. Role of sea surface temperature, arctic sea ice and
543 siberian snow in forcing the atmospheric circulation in winter of 2012–2013. *Climate*
544 *Dynamics* 45, 1181–1206.
- 545 Rasmijn, L., Van der Schrier, G., Bintanja, R., Barkmeijer, J., Sterl, A., Hazeleger, W.,

546 2018. Future equivalent of 2010 russian heatwave intensified by weakening soil moisture
547 constraints. *Nature Climate Change* 8, 381–385.

548 Rayner, N., Parker, D.E., Horton, E., Folland, C.K., Alexander, L.V., Rowell, D., Kent, E.,
549 Kaplan, A., 2003. Global analyses of sea surface temperature, sea ice, and night marine
550 air temperature since the late nineteenth century. *Journal of Geophysical Research:*
551 *Atmospheres* 108.

552 Ren, X., Zhang, L., Cai, W., Li, X., Wang, C.Y., Jin, Y., Wu, L., 2022. Influence of
553 tropical atlantic meridional dipole of sea surface temperature anomalies on antarctic
554 autumn sea ice. *Environmental Research Letters* 17, 094046.

555 Robine, J.M., Cheung, S.L.K., Le Roy, S., Van Oyen, H., Griffiths, C., Michel, J.P.,
556 Herrmann, F.R., 2008. Death toll exceeded 70,000 in europe during the summer of
557 2003. *Comptes rendus biologiques* 331, 171–178.

558 Rudeva, I., Simmonds, I., 2021. Midlatitude winter extreme temperature events and
559 connections with anomalies in the arctic and tropics. *Journal of Climate* 34, 3733–3749.

560 Runge, J., Nowack, P., Kretschmer, M., Flaxman, S., Sejdinovic, D., 2019. Detecting and
561 quantifying causal associations in large nonlinear time series datasets. *Science advances*
562 5, eaau4996.

563 Russo, S., Sillmann, J., Fischer, E.M., 2015. Top ten european heatwaves since 1950 and
564 their occurrence in the coming decades. *Environmental Research Letters* 10, 124003.

565 Sardeshmukh, P.D., Hoskins, B.J., 1988. The generation of global rotational flow by steady
566 idealized tropical divergence. *Journal of the Atmospheric Sciences* 45, 1228–1251.

567 Schneidereit, A., Schubert, S., Vargin, P., Lunkeit, F., Zhu, X., Peters, D.H., Fraedrich,
568 K., 2012. Large-scale flow and the long-lasting blocking high over Russia: Summer 2010.
569 *Monthly Weather Review* 140, 2967–2981.

570 Schubert, S.D., Wang, H., Koster, R.D., Suarez, M.J., Groisman, P.Y., 2014. Northern
571 eurasian heat waves and droughts. *Journal of Climate* 27, 3169–3207.

572 Schumacher, D.L., Keune, J., Van Heerwaarden, C.C., Vilà-Guerau de Arellano, J., Teul-
573 ing, A.J., Miralles, D.G., 2019. Amplification of mega-heatwaves through heat torrents
574 fuelled by upwind drought. *Nature Geoscience* 12, 712–717.

575 Simmonds, I., 2018. What causes extreme hot days in europe? *Environmental Research*
576 *Letters* 13.

577 Strigunova, I., Blender, R., Lunkeit, F., Žagar, N., 2022. Signatures of eurasian heat waves
578 in global rossby wave spectra. *Weather and Climate Dynamics* 3, 1399–1414.

579 Sun, C., Li, J., Ding, R., 2016. Strengthening relationship between enso and western
580 russian summer surface temperature. *Geophysical Research Letters* 43, 843–851.

581 Takaya, K., Nakamura, H., 2001. A formulation of a phase-independent wave-activity flux
582 for stationary and migratory quasigeostrophic eddies on a zonally varying basic flow.
583 *Journal of the Atmospheric Sciences* 58, 608–627.

584 Toniazzo, T., Scaife, A.A., 2006. The influence of enso on winter north atlantic climate.
585 Geophysical Research Letters 33.

586 Trenberth, K.E., Fasullo, J.T., 2012. Climate extremes and climate change: The rus-
587 sian heat wave and other climate extremes of 2010. Journal of Geophysical Research:
588 Atmospheres 117.

589 Tyrlis, E., Hoskins, B., 2008. Aspects of a northern hemisphere atmospheric blocking
590 climatology. Journal of the atmospheric sciences 65, 1638–1652.

591 Vecchi, G.A., Delworth, T., Gudgel, R., Kapnick, S., Rosati, A., Wittenberg, A.T., Zeng,
592 F., Anderson, W., Balaji, V., Dixon, K., et al., 2014. On the seasonal forecasting of
593 regional tropical cyclone activity. Journal of Climate 27, 7994–8016.

594 Velikou, K., Lazoglou, G., Tolika, K., Anagnostopoulou, C., 2022. Reliability of the era5
595 in replicating mean and extreme temperatures across europe. Water 14, 543.

596 Vimont, D.J., Kossin, J.P., 2007. The atlantic meridional mode and hurricane activity.
597 Geophysical Research Letters 34.

598 Vittal, H., Villarini, G., Zhang, W., 2020a. Early prediction of the indian summer monsoon
599 rainfall by the atlantic meridional mode. Climate dynamics 54, 2337–2346.

600 Vittal, H., Villarini, G., Zhang, W., 2020b. On the role of the atlantic ocean in exacerbating
601 indian heat waves. Climate dynamics 54, 1887–1896.

- 602 Wang, C., 2004. Enso, atlantic climate variability, and the walker and hadley circulations,
603 in: *The Hadley circulation: Present, past and future*. Springer, pp. 173–202.
- 604 Welbergen, J.A., Klose, S.M., Markus, N., Eby, P., 2008. Climate change and the effects
605 of temperature extremes on australian flying-foxes. *Proceedings of the Royal Society B:
606 Biological Sciences* 275, 419–425.
- 607 Wilks, D.S., 2011. *Statistical methods in the atmospheric sciences*. volume 100. Academic
608 press.
- 609 Williams, A.P., Cook, E.R., Smerdon, J.E., Cook, B.I., Abatzoglou, J.T., Bolles, K., Baek,
610 S.H., Badger, A.M., Livneh, B., 2020. Large contribution from anthropogenic warming
611 to an emerging North American megadrought. *Science* 368, 314–318. doi:10.1126/
612 science.aaz9600.
- 613 Wittenberg, A.T., Vecchi, G.A., Delworth, T.L., Rosati, A., Anderson, W.G., Cooke,
614 W.F., Underwood, S., Zeng, F., Griffies, S.M., Ray, S., 2018. Improved simulations of
615 tropical pacific annual-mean climate in the gfdl flor and hiflor coupled gcms. *Journal of
616 Advances in Modeling Earth Systems* 10, 3176–3220.
- 617 Wunsch, C., 1999. The interpretation of short climate records, with comments on the
618 North Atlantic and Southern Oscillations. *Bulletin of the American Meteorological
619 Society* 80, 245–256.
- 620 Xie, L., Yan, T., Pietrafesa, L.J., Morrison, J.M., Karl, T., 2005. Climatology and inter-
621 annual variability of north atlantic hurricane tracks. *Journal of climate* 18, 5370–5381.

- 622 Zhang, R., Sun, C., Zhu, J., Zhang, R., Li, W., 2020. Increased european heat waves in
623 recent decades in response to shrinking arctic sea ice and eurasian snow cover. *NPJ*
624 *Climate and Atmospheric Science* 3, 1–9.
- 625 Zhang, W., Vecchi, G.A., Murakami, H., Villarini, G., Jia, L., 2016. The pacific meridional
626 mode and the occurrence of tropical cyclones in the western north pacific. *Journal of*
627 *Climate* 29, 381–398.
- 628 Zhang, W., Vecchi, G.A., Villarini, G., Murakami, H., Rosati, A., Yang, X., Jia, L., Zeng,
629 F., 2017. Modulation of western north pacific tropical cyclone activity by the atlantic
630 meridional mode. *Climate Dynamics* 48, 631–647.
- 631 Zhao, W., Zhou, N., Chen, S., 2020. The record-breaking high temperature over europe
632 in june of 2019. *Atmosphere* 11, 524.

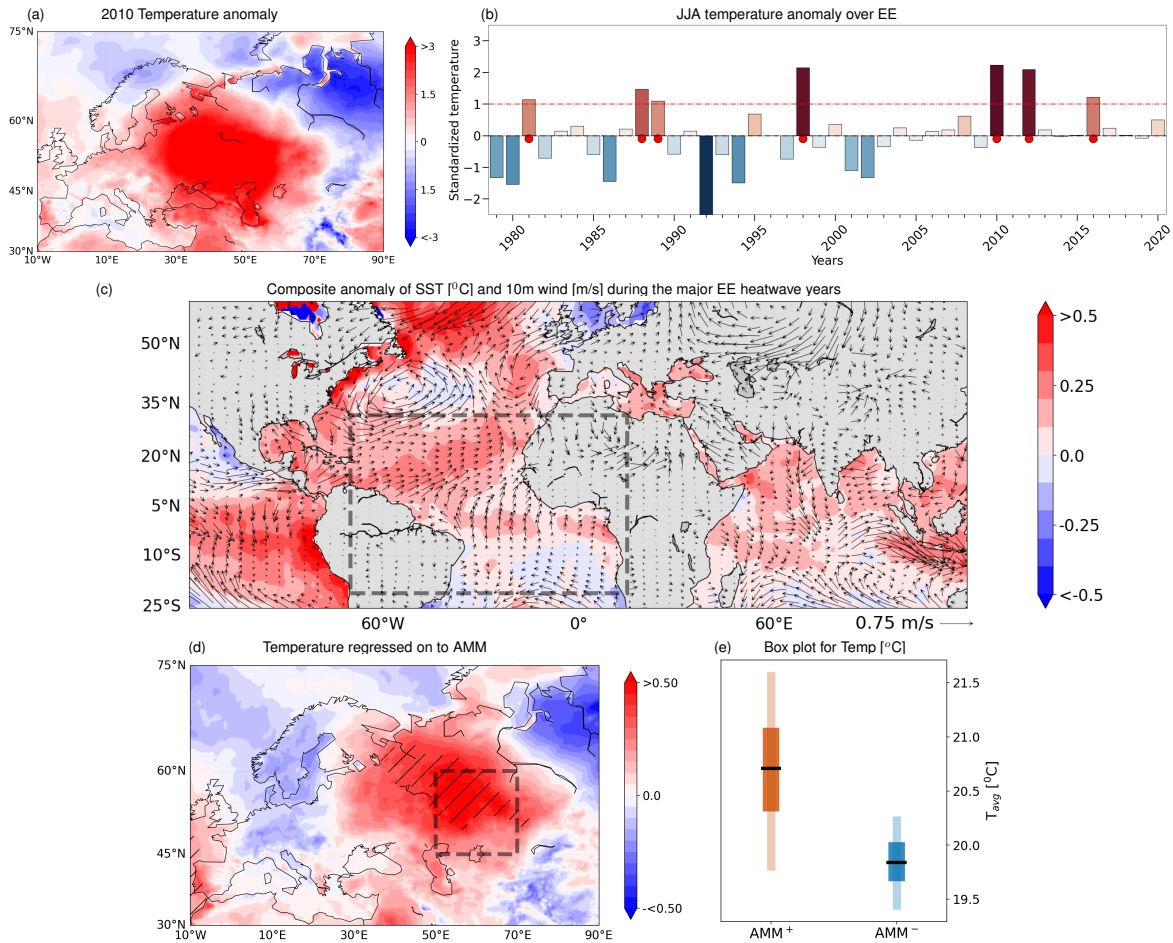


Figure 1: **Summer temperature variability (June–August) across the eastern European region and corresponding large-scale atmospheric and sea surface dynamics** (a) Surface temperature anomaly over the European region during the summer of 2010 – which is one of the most severe heatwave summers in the eastern European region. (b) Inter-annual variability of summer temperature anomalies (anomalies with respect to the climatological mean) over the eastern European region (50°E – 70°E and 45°N – 60°N ; shown in rectangular box in d). The positive (negative) anomalies are represented by blue (red) color. The positive one standard deviation value is indicated by the red dashed line. (c) Composites of the SST ($^{\circ}\text{C}$) and surface wind anomalies corresponding to the major heatwave years over eastern European region (red dots in the panel b). The black rectangular box in panel (c) over the tropical Atlantic Ocean (75°E – 15°E and 21°S – 32°N) represents the core Atlantic Meridional Mode (AMM) region. The spatial pattern of both SST and wind in this region reveal the dominant positive phase of the AMM. (d) Regression of summer temperature over Europe onto leading AMM index during the period 1980–2019. The hatched areas represent the locations where the slopes are significant at the 5% level. (e) Box plot showing the differences in temperature in the eastern European temperature between the positive and negative phases of AMM.

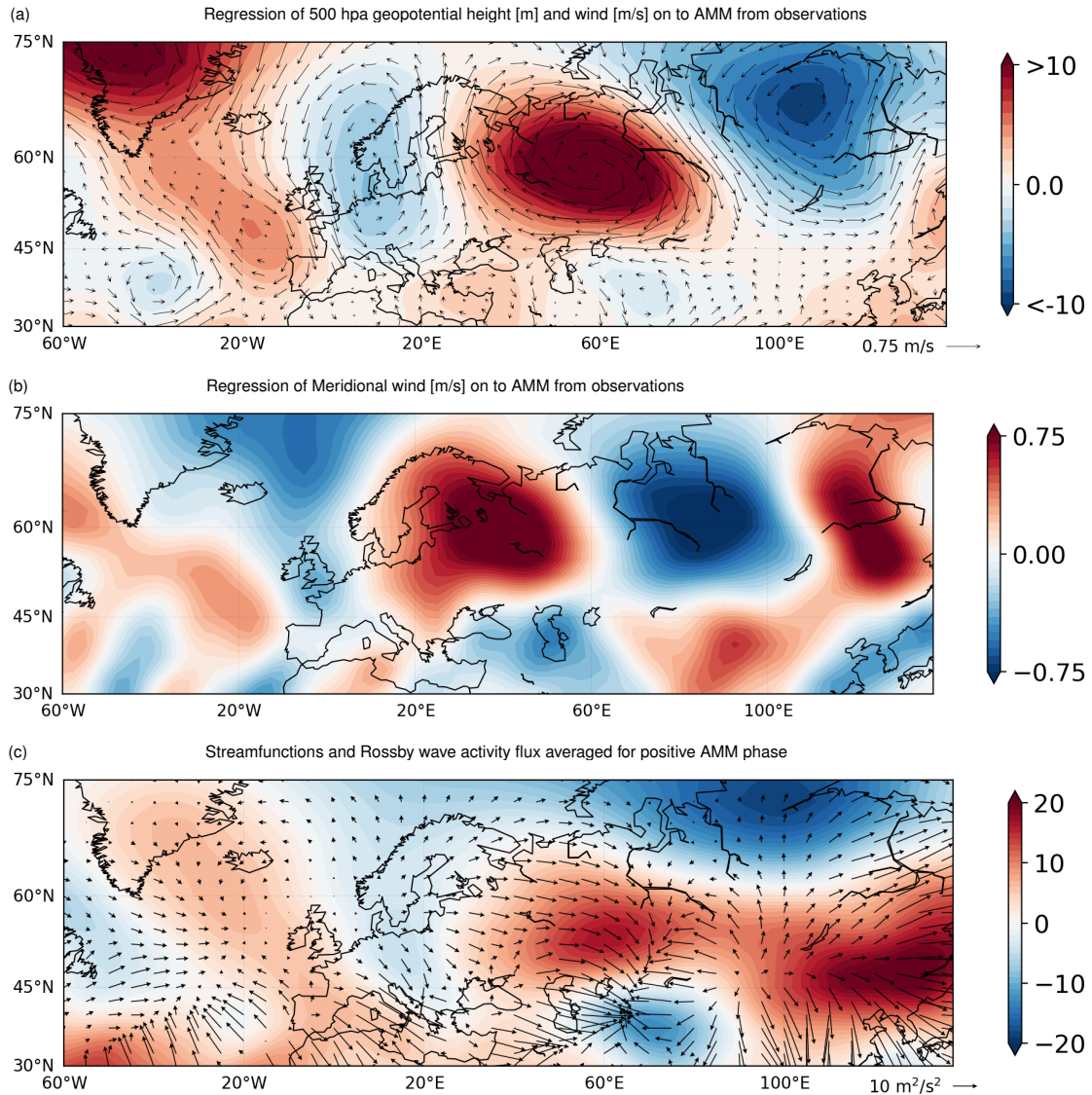


Figure 2: **Large-scale controls of AMM on the eastern European summer (June–August) heatwave variability from observations.** (a) Large-scale atmospheric circulation pattern associated with the AMM in terms of the regression of 500 hPa geopotential height (shading) and winds (vectors) from NCEP reanalysis during 1951–2020. (b) The meridional wind response to the AMM during the summers from 1951–2020. (c) Same as (b) but for streamfunction and wave activity flux (WAF). We present the averaged WAF for those summers with increased (positive phase) AMM summers.

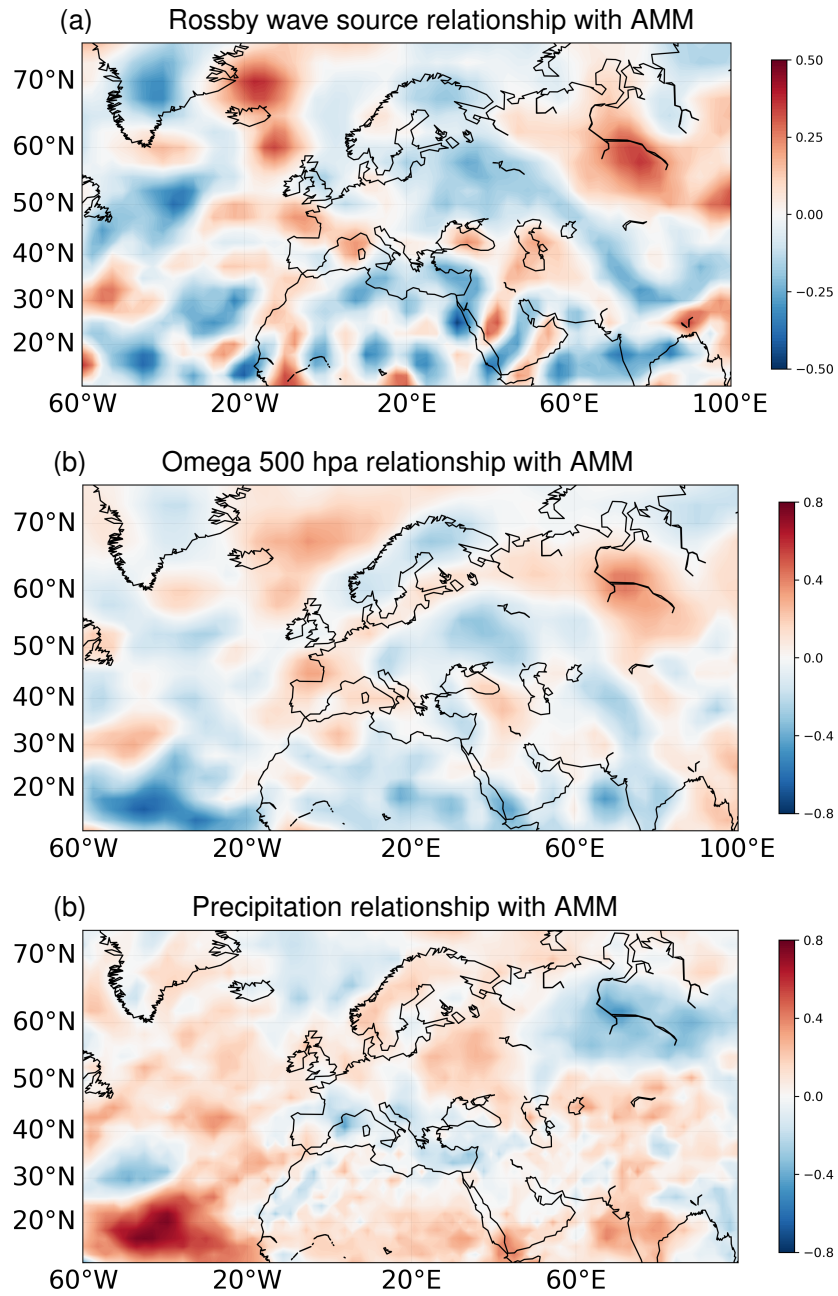


Figure 3: Correlation maps of (a) Summer Rossby wave source at 200 hPa level (b) summer 500 hPa omega and summer precipitation (c) with the summer AMM index from 1951–2019.

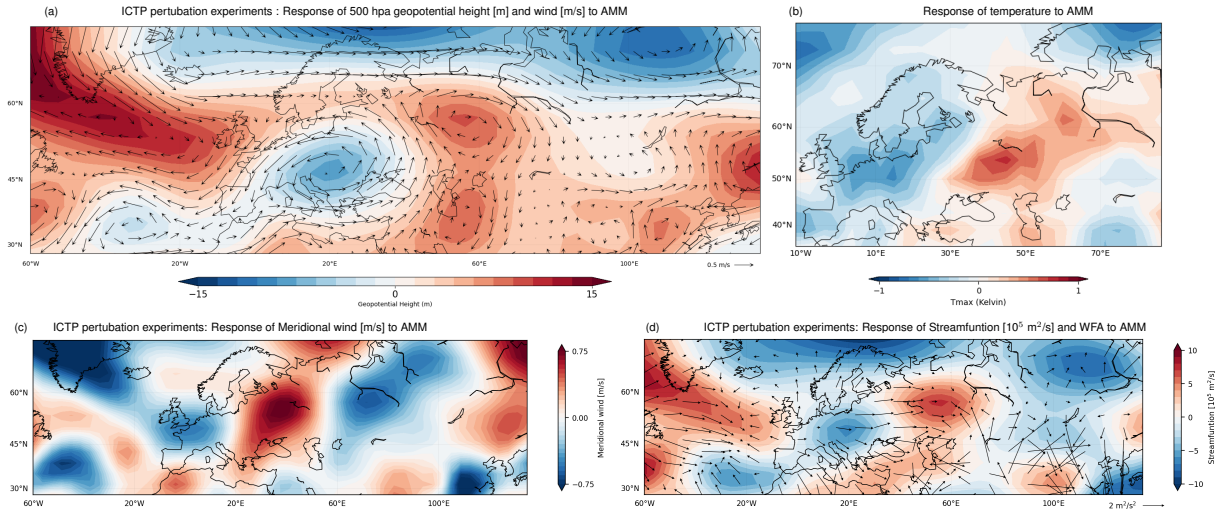


Figure 4: **Representation of AMM forcing mechanisms on the eastern European temperature variability in a perturbation climate model experiment.** (a) large-scale atmospheric circulation response to the AMM based on an ICTP climate model perturbation experiment (25 yr of simulation). (b) Temperature response over Europe to the AMM based on ICTP climate model perturbation experiment. (c) The meridional wind response to the AMM during the summers from the ICTP experiment. (d) Same as (c) but for streamfunction and wave activity flux (WAF). We present the averaged WAF for the perturbed experiment only whereas the streamfunction is the difference between the perturbed and CLIM experiments (See method for more details).

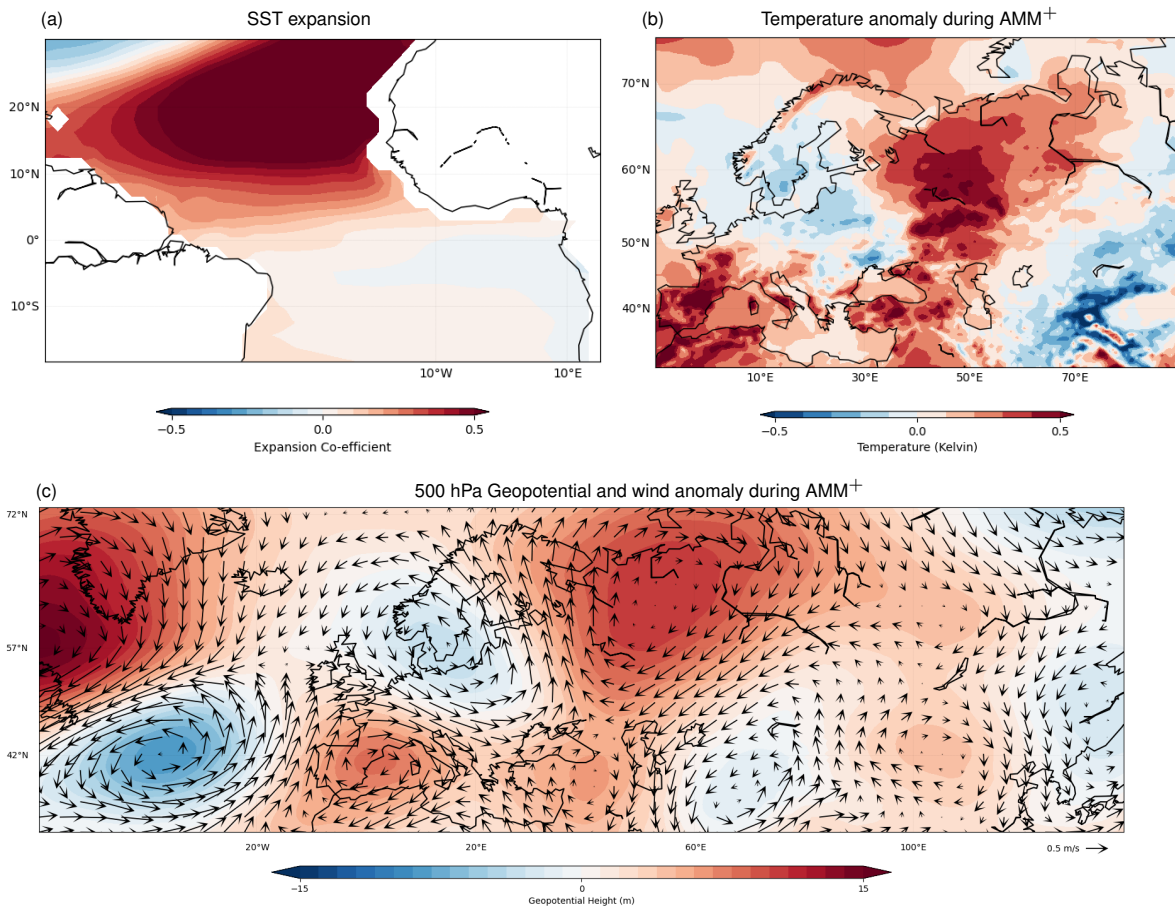


Figure 5: Representation of AMM forcing mechanisms on the EE temperature variability in a climate model control experiment. (a) The GFDL FLOR control model is able to represent the SST expansion mode of the AMM. (b) Temperature response over Europe to the AMM based on climate model control experiment. (c) Large-scale atmospheric circulation response to the AMM based on GFDL FLOR climate model control experiment (300 yr of simulation).

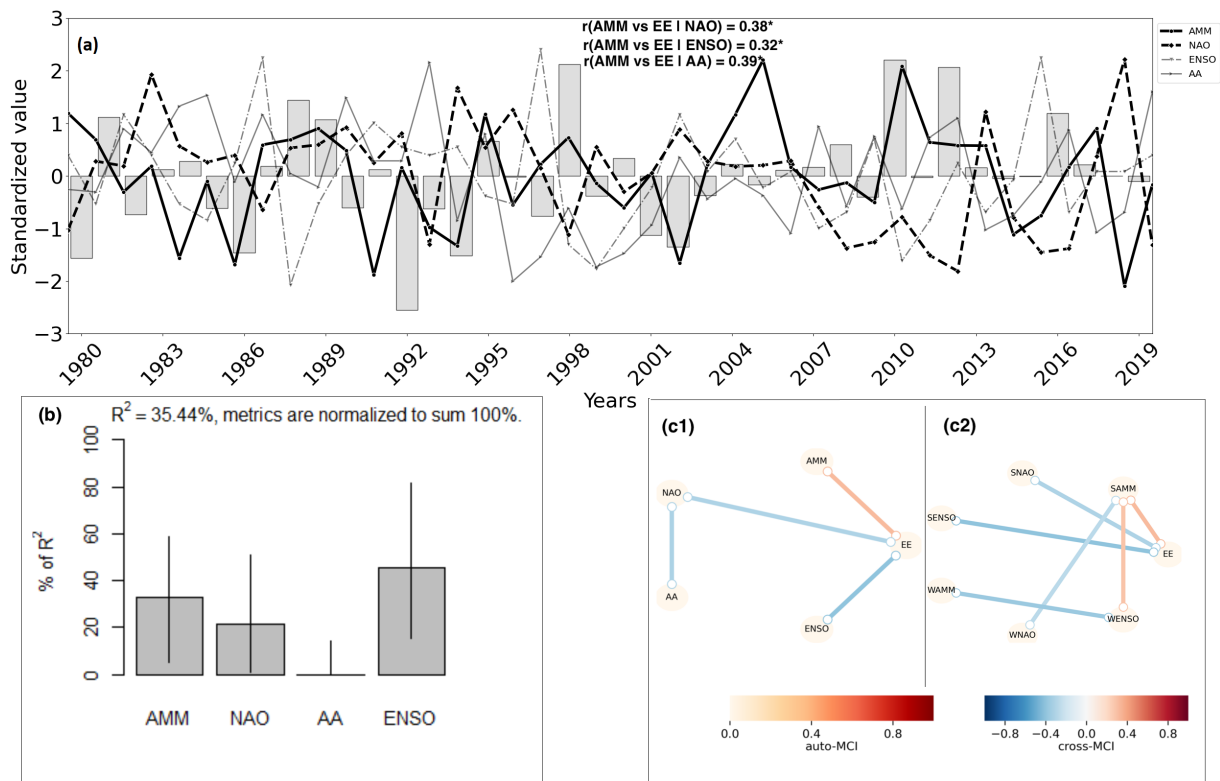


Figure 6: **Relation of EE temperature with other important climate modes during summer.** (a) Inter-annual variability of the leading AMM index and temperature over the EE region (represented with the bar plot) during summer, with variability being represented in terms of their standardized scores. Along with AMM, we also represent other important climatic modes, such as NAO, ENSO and AA – all these being represented with standardized values. We notice that the identified linkages between the AMM and EE temperature variability are robust even in the presence of these large-scale climate modes – represented with partial correlation analysis (provided in the inset of the figure wherein the p-value ≤ 0.05 is represented with “*” symbol). (b) Relative importance analysis of the large-scale climatic modes on the EE temperature variability. (c1) Causal links between the EE temperature variability and the summer AMM with the presence of some other important drivers (during the summer months) using the PCMCI+ causal inference framework at 95% alpha level. (c2) We also considered the SST modes during the preceding winter season (represented with W, for example, the winter AMM is represented with WAMM and for the summer, it is with SAMM. Similar for other considered climatic modes) and their effect on the summer EE temperature variability along with the summer season. The correlation between SAMM and WENSO is 0.28 and SAMM and WNAO is -0.27 and these are significant at 5% level